IEEE Access
Multidisciplinary | Rapid Review | Open Access Journal

Received October 23, 2020, accepted November 20, 2020, date of publication November 25, 2020,
date of current version December 10, 2020.

Digital Object Identifier 10.1109/ACCESS.2020.3040378

Design of Weakly-Coupled 16-Vector-Mode Coaxial Bragg FMF for Short-Haul Communication

YIYING ZHANG[1], FANG REN[1,2], XIAOJIE FAN[1], JINYU ZHANG[1], JINGJING NIU[1], AND JIANPING WANG[1,2]

[1]School of Computer and Communication Engineering, University of Science and Technology Beijing, Beijing 100083, China
[2]Beijing Engineering and Technology Research Center for Convergence Networks and Ubiquitous Services, University of Science and Technology Beijing, Beijing 100083, China

Corresponding author: Fang Ren (renfang@ustb.edu.cn)

This work was supported in part by the Fundamental Research Funds for the Central University, China, under Grant FRF-BD-20-11A, and in part by the National Natural Science Foundation of China (NSFC) under Grant 61671055.

ABSTRACT Utilizing weakly-coupled few-mode-fibers (FMFs) for MIMO-DSP eliminating in short-haul mode division multiplexing(MDM) systems has attracted much attention recently, as an effective solution to suppress modal crosstalk. In this article, we propose a weakly-coupled 16-vector-mode coaxial Bragg FMF supporting 16 vector modes(HE_{11a}, HE_{11b}, TM_{01}, HE_{21a}, HE_{21b}, TE_{01}, HE_{31a}, HE_{31b}, EH_{11a}, EH_{11b}, HE_{12a}, HE_{12b}, EH_{21a}, EH_{21b}, HE_{41a}, HE_{41b}) which works across the C-band and explore the possibility for weakly-coupled Bragg FMFs. We optimize the geometric parameters and evaluate their effects on modal n_{eff}, $min\Delta n_{eff}$, and A_{eff}. The DMD, modal confinement loss and bending loss are also investigated. The simulation results indicate that the proposed fiber can obtain large $min\Delta n_{eff}$ between adjacent vector modes ($\sim 2 \times 0.0001$), and can be a promising candidate for MIMO-DSP simplified short-haul MDM transmission systems.

INDEX TERMS Mode division multiplexing, short-haul communication, weakly-coupled, few-mode Bragg fiber.

I. INTRODUCTION

As the single-mode fiber (SMF) transmission system is facing the approaching of Shannon limit, the mode division multiplexing (MDM) transmission with few-mode fibers (FMFs) is considered to be a promising future solution of the capacity crunch. Dealing with modal crosstalk caused by modal coupling is a core issue for MDM systems. Using the multi-input-multi-output digital signal processing (MIMO-DSP) for compensating crosstalk is suitable for long-haul scenarios, however the computation complexity and cost are burdensome and not acceptable for the rapidly developing short-haul MDM transmission systems[1]. Therefore, weakly-coupled FMFs with large effective index difference (Δn_{eff}) between adjacent modes have been suggested for modal coupling suppression in short-haul MDM systems, in which the signals of adjacent modes can be transmitted independently. Among weakly-coupled FMFs, several design schemes such as FMFs with ring-core [2],[3], elliptical core [4], or stress region for polarization maintaining [5] have been carried out. These fibers mainly work at 1550nm and require little or none MIMO-DSP in the transmission systems.

The Bragg fibers achieve light confinement through the photonic bandgap by its periodic cladding of alternating high and low refractive indices. This concept was first proposed by Yeh *et al* [6]. Theoretical analyses using other methods such as the asymptotic analysis were carried out after that [7]–[11]. Bragg fibers have the appealing features of low dispersion [9], low radiation loss [10], and the possibility of guiding light in an air core [14]–[17]. Adjusting the properties of such fibers can obtain various characteristics for various scenarios, such as dispersion management [18] or mode selection [19] for transmission, and fiber sensor [20]–[22] or laser [23] for fiber optical devices. Several reports on Bragg fibers as transmission waveguides have been carried out recently. Y. J. Yehouessi *et al.* reported an all-solid Bragg fiber with the effective mode area of about 3700 μm^2 at 1035 nm by using a pixelated Bragg fiber geometry [24]; M. Shang *et al.* introduced two air holes into the core of an all-solid Bragg fiber to produce high birefringence [25]; X. Bai *et al.* proposed a Bragg fiber with dual claddings, which can support 50 OAM modes [26]. The study of Bragg fibers as weakly-coupled FMFs is still a shortage, to our knowledge.

The associate editor coordinating the review of this manuscript and approving it for publication was Barbara Masini.

Bragg fibers with a high index dielectric medium core are called the coaxial Bragg fibers. The concept of coaxial Bragg fibers came from the analogy between dielectric coaxial fibers and metallic coaxial cables. Coaxial fibers have better performance of light confinement while possessing the same light-guiding mechanism as ordinary Bragg fibers. The all-dielectric single-mode coaxial Bragg fiber was first proposed by Ihanescu *et al* [27] to study its dispersion and polarization rotation performance in high-data-rate scenarios, while later researches have not given full consideration to coaxial Bragg fibers for few-mode applications. Over all, the Bragg fiber has the potential of applying to few-mode short-haul transmission, owing to its large effective index differences between adjacent propagation modes, yet few studies have been carried out on few-mode Bragg fibers, let alone coaxial Bragg fibers.

In this article, we mainly propose a weakly-coupled 16-vector-mode coaxial Bragg FMF supporting 16 vector modes. We carry out numerical simulations to investigate the influence of fiber parameters on its effective refractive index (n_{eff}), minimal Δn_{eff} ($min\Delta n_{eff}$), and modal effective area (A_{eff}). We also evaluate the differential mode delay, modal confinement loss and bending effect of propagation modes. Simulation results show that by optimization, the weakly-coupled few-mode Bragg fiber can be achieved with large $min\Delta n_{eff}$ of around 0.0002 between adjacent spatial modes at 1550nm. The proposed fiber has potential for applying to short-haul MDM communication systems such as passive optical network (PON), datacenter network and optical interconnections for MIMO-DSP simplifying and optical sensing devices.

II. METHODS

A. FIBER STRUCTURE AND PARAMETERS OF THE COAXIAL BRAGG FMF

We design a weakly-coupled coaxial Bragg FMF supporting 16 vector modes with the parameters shown in Fig. 1. The fiber structure includes several periodic layers of alternating refractive indices with width l, an air core with radius r and a central circular dielectric medium with radius d and refractive index n_c, and the refractive index (RI) difference Δn_1 between the high-index and low-index layers. The width of each high-index layer l_1 makes up 0.33 of l in terms of proportion, and the refractive indices of high and low index parts are set to be 4.58 and 1.55 (at 1550nm), by which a single-mode Bragg fiber has been fabricated, according to previous works [27]–[30]. The fiber characteristics are simulated with finite element method (FEM) methods. The large refractive index difference between cladding layers is large enough to form rather wide photonic bandgap and therefore is beneficial for light guiding [29]. Schematics of cross section and refractive index profile for the proposed fiber are shown in Fig. 1(a), (b).

The Bragg FMF is added with the central dielectric medium to confine light in the air core better [31], and what's more to further separate vector modes. An ordinary hollow

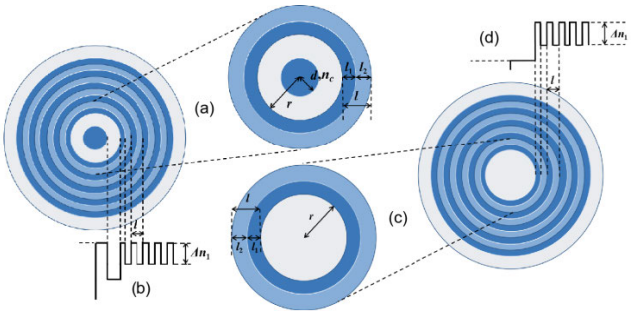

FIGURE 1. Fiber structure and parameters of the designed coaxial Bragg FMF and an ordinary air-core Bragg FMF. (a) Schematic of cross section in the coaxial Bragg FMF; (b) Schematic of refractive index profile in the coaxial Bragg FMF; (c) Schematic of cross section in the hollow Bragg FMF; (d) Schematic of refractive index profile in the hollow Bragg FMF. The deeper color represents higher refractive index.

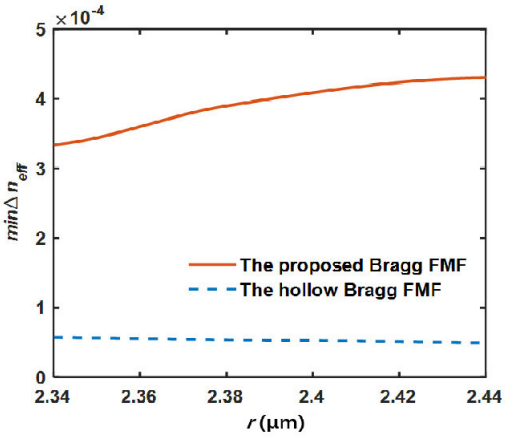

FIGURE 2. Variation of $\min\Delta n_{eff}$ as a function of air core radius r in the proposed coaxial Bragg FMF and an ordinary hollow Bragg FMF.

Bragg FMF is designed to contrast the $min\Delta n_{eff}$ between adjacent modes with the proposed fiber. Schematics of cross section and refractive index profile for the hollow Bragg FMF are shown in Fig. 1(c) and (d), with parameters of l, l_1, l_2, r and Δn_1. Where l stands for the width of the high(l_1) and low(l_2) index layers of the cladding, r is the radius of the air core, and Δn_1 represents the RI difference between the layer refractive indices. Fig. 2 shows the curves of $\min\Delta n_{eff}$ as a function of r in the proposed Bragg FMF and an ordinary hollow Bragg FMF when material, air core size r, Bragg layer numbers and layer width l of these two kinds of fibers are set as the same. The results in Fig.2 indicate that for the hollow fiber, the $min\Delta n_{eff}$ of the desired modes is around 5×10^{-5}, while that of the proposed FMF exceeds 10^{-4}, which means the latter has a better performance in terms of separating adjacent eigenmodes. Therefore, the coaxial center structure is better for air-core Bragg FMFs to more fully utilize eigenmodes and improve the transmission capacity.

B. ELECTROMAGNETIC FIELD DISTRIBUTIONS OF THE COAXIAL BRAGG FMF

As has been studied in [10] by asymptotic matrix formalism, the electromagnetic fields in a Bragg fiber can be separated into two parts: the core region and the cladding region. In this

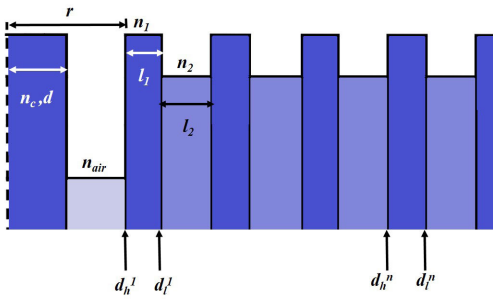

FIGURE 3. Schematic of the cross section of the proposed Bragg fiber. In the cladding region, the high-index layer has the thickness of l_1 and refractive index n_1, while the low-index layer has the thickness of l_2 and refractive index n_2.

article, the core region is composed of the central dielectric medium cylinder, and the air core. Schematic of the cross section of the proposed Bragg fiber is shown in Fig. 3. The electromagnetic field intensity in the central dielectric medium is supposed to be low. Using the Maxwell equations, the transverse field components in the air core region can be represented by H_z and E_z in formula (1) - (4).

$$E_r = \frac{i\beta}{(\frac{\omega^2}{c^2})n^2 - \beta^2}(\frac{\partial}{\partial r}E_z + \frac{\omega\mu_0}{\beta}\frac{\partial}{r\partial\theta}H_z) \quad (1)$$

$$E_\theta = \frac{i\beta}{(\frac{\omega^2}{c^2})n^2 - \beta^2}(\frac{\partial}{r\partial\theta}E_z - \frac{\omega\mu_0}{\beta}\frac{\partial}{\partial r}H_z) \quad (2)$$

$$H_r = \frac{i\beta}{(\frac{\omega^2}{c^2})n^2 - \beta^2}(-\frac{\omega\varepsilon_0 n^2}{\beta}\frac{\partial}{r\partial\theta}E_z + \frac{\partial}{\partial r}H_z) \quad (3)$$

$$H_\theta = \frac{i\beta}{(\frac{\omega^2}{c^2})n^2 - \beta^2}(\frac{\omega\varepsilon_0 n^2}{\beta}\frac{\partial}{\partial r}E_z + \frac{\partial}{r\partial\theta}H_z) \quad (4)$$

The general solutions of $Ez(\theta)$ and $H_z(\theta)$ can be given by the superposition of Bessel functions. Here we use the Bessel functions $Jm(kr)$ and $Ym(kr)$, where r means the distance from the center of the circle to the edge of core ($r \geq d$) for each m.

$$\begin{bmatrix} E_z \\ \frac{1}{i\beta}H_\theta \\ H_z \\ -\frac{1}{i\beta}E_\theta \end{bmatrix} = M(n_{air}, k_{air}, r)\begin{bmatrix} A_i \\ B_i \\ C_i \\ D_i \end{bmatrix} \quad (5)$$

where $n_{air} = 1$ and $k_{air} = ((n_{air}\omega/c)^2 - \beta^2)^{1/2} = ((\omega/c)^2 - \beta^2)^{1/2}$, A_i, B_i, C_i, D_i are constants, and M is defined as formula (6) at the bottom of the page.

For the cladding region, the high-index layer has the thickness of l_1 and refractive index n_1, while the low-index layer has the thickness of l_2 and refractive index n_2. As shown in Fig. 3, $d_h^n \leq r < d_h^n + l_1$ denotes the high-index region and $d_l^n \leq r < d_l^n + l_2$ denotes the low-index region. When the TM and TE components are regarded as decoupled with each other, with amplitudes of A_{TM} and A_{TE} respectively, the field distributions can be described as:

$$E_z = \begin{cases} \frac{A_{TM}}{\sqrt{k_1 r}}\left[a_n e^{ik_1(r-d_h^n)} + b_n e^{-ik_1(r-d_h^n)}\right] \\ \qquad d_h^n \leq r < d_h^n + l_1 \\ \frac{A_{TM}}{\sqrt{k_2 r}}\left[a'_n e^{ik_2(r-d_l^n)} + b'_n e^{-ik_2(r-d_l^n)}\right] \\ \qquad d_l^n \leq r < d_l^n + l_2 \end{cases} \quad (7)$$

$$E_\theta = \begin{cases} \frac{\omega\mu_0}{k_1}\frac{A_{TE}}{\sqrt{k_1 r}}\left[c_n e^{ik_1(r-d_h^n)} - d_n e^{-ik_1(r-d_h^n)}\right] \\ \qquad d_h^n \leq r < d_h^n + l_1 \\ \frac{\omega\mu_0}{k_2}\frac{A_{TE}}{\sqrt{k_2 r}}\left[c'_n e^{ik_2(r-d_l^n)} + d'_n e^{-ik_2(r-d_l^n)}\right] \\ \qquad d_l^n \leq r < d_l^n + l_2 \end{cases} \quad (8)$$

$$H_z = \begin{cases} \frac{A_{TE}}{\sqrt{k_1 r}}\left[c_n e^{ik_1(r-d_h^n)} + d_n e^{-ik_1(r-d_h^n)}\right] \\ \qquad d_h^n \leq r < d_h^n + l_1 \\ \frac{A_{TE}}{\sqrt{k_2 r}}\left[c'_n e^{ik_2(r-d_l^n)} + d'_n e^{-ik_2(r-d_l^n)}\right] \\ \qquad d_l^n \leq r < d_l^n + l_2 \end{cases} \quad (9)$$

$$H_\theta = \begin{cases} -\frac{\omega\varepsilon_0 n_1^2}{k_1}\frac{A_{TM}}{\sqrt{k_1 r}}\left[a_n e^{ik_1(r-d_h^n)} + b_n e^{-ik_1(r-d_h^n)}\right] \\ \qquad d_h^n \leq r < d_h^n + l_1 \\ -\frac{\omega\varepsilon_0 n_2^2}{k_2}\frac{A_{TM}}{\sqrt{k_2 r}}\left[a'_n e^{ik_2(r-d_l^n)} + b'_n e^{-ik_2(r-d_l^n)}\right] \\ \qquad d_l^n \leq r < d_l^n + l_2 \end{cases} \quad (10)$$

Using the boundary conditions, as when $E_z(\theta)$ and $H_z(\theta)$ are continuous at the edge of each layer, the fields in both core and cladding region can be described by the asymptotic approximation.

C. OPTIMIZATION OF THE COAXIAL BRAGG FMF

The proposed fiber is supposed to support 16 vector modes (HE_{11a}, HE_{11b}, TM_{01}, HE_{21a}, HE_{21b}, TE_{01}, HE_{31a}, HE_{31b}, EH_{11a}, EH_{11b}, HE_{12a}, HE_{12b}, EH_{21a}, EH_{21b}, HE_{41a}, HE_{41b}). The $min\Delta n_{eff}$ between two adjacent modes must be larger than 10^{-4} to suppress modal coupling [32]. The modal

$$M(n_{air}, k_{air}, r) = \begin{bmatrix} J_m(k_{air}r) & Y_m(k_{air}r) & 0 & 0 \\ \frac{\omega\varepsilon_0 n_{air}^2}{k_{air}\beta}J'_m(k_{air}r) & \frac{\omega\varepsilon_0 n_{air}^2}{k_{air}\beta}Y'_m(k_{air}r) & \frac{m}{k_{air}^2 r}J_m(k_{air}r) & \frac{m}{k_{air}^2 r}Y_m(k_{air}r) \\ 0 & 0 & J_m(k_{air}r) & Y_m(k_{air}r) \\ \frac{m}{k_{air}^2 r}J_m(k_{air}r) & \frac{m}{k_{air}^2 r}Y_m(k_{air}r) & \frac{\omega\mu_0}{k_{air}\beta}J'_m(k_{air}r) & \frac{\omega\mu_0}{k_{air}\beta}Y'_m(k_{air}r) \end{bmatrix} \quad (6)$$

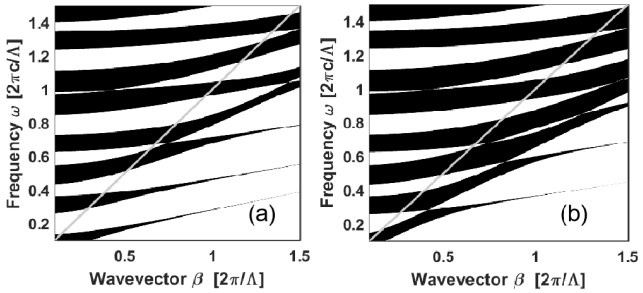

FIGURE 4. The bandgap structure of the coaxial Bragg FMF when l_1/l is set to be 0.33. (a)TE bandgap structure; (b)TM bandgap structure. The white regions represent for the bandgap region. The gray lines represent the air light line.

properties of the proposed fiber can be adjusted by operating the geometrical parameters shown in Fig. 1.

Bragg fibers confine light in the low-index core by generating bandgap effects in the periodic cladding rather than total internal reflection [9]. In order to support more higher-order modes, the confinement losses of several modes are larger than that of a single-mode Bragg fiber. Figure 4 shows the first few TE and TM bandgaps of the proposed Bragg fiber when the high-index layer width l_1 accounts for 0.33 of each alternating layer l, and the effective refractive indices of the layers are fixed to be 4.58 for high-index regions and 1.55 for low-index regions at 1550nm. As is shown in Fig. 4, the TE mode bandgap is wider than that of the TM mode, so we only consider the latter during optimization. The surface-parallel wavevector component β and the frequency ω are expressed in the unit of $2\pi/\Lambda$ and $2\pi c/\Lambda$, respectively, where Λ represents the width of each alternating layer (1 high-index layer and 1 low-index layer) l. The white regions are the bandgap regions, among which light can propagate in the air. We choose the 6th bandgap in Fig. 4(b), where the vertical axis $\omega/(2\pi c/\Lambda) \approx 1.2$, and Λ sets at (1.7-1.95) μm. For the convenience of fabrication, we keep one decimal fraction and choose l to be 1.8 or 1.9μm. It needs to be noticed that the center high-index core plays the vital role when the guided modes pass the air light line [31].

For Bragg fibers, high-order modes may also exist in the fiber until they fade away after several miles of transmission. Our aim is to make the proposed fiber support up to 16 vector modes, so we have to sacrifice some loss performance, therefore the maximum confinement loss of the proposed fiber is not as good compared with a single-mode Bragg fiber of the previous work [33], which also means that the confinement loss of the proposed fiber is not suitable for long-haul transmission scenarios. In terms of the proposed 16-mode FMF, the modes of more than 17th have the confinement loss of exceeding 10^3 dB/m, while the confinement loss of the desired 16 modes can be less than 10^2 dB/m as will be shown later in Fig. 10, so we suppose the loss of the former to be too large to satisfy the propagation condition, or in other words, to be cut-off.

The confinement loss L_c (dB/m) of each mode can be calculated through the imaginary part of each mode's effective mode index $Im(n_{eff})$ [34].

$$L_c = [40\pi \cdot Im(n_{eff})]/[\ln(10)\lambda] \tag{11}$$

Fig. 5 presents the variation of n_{eff} as a function of the air core radius r with the periodic layer width $l = 1.8$, 1.85 and 1.9μm, when d/r is fixed to be 0.1 and l_1/l is fixed to

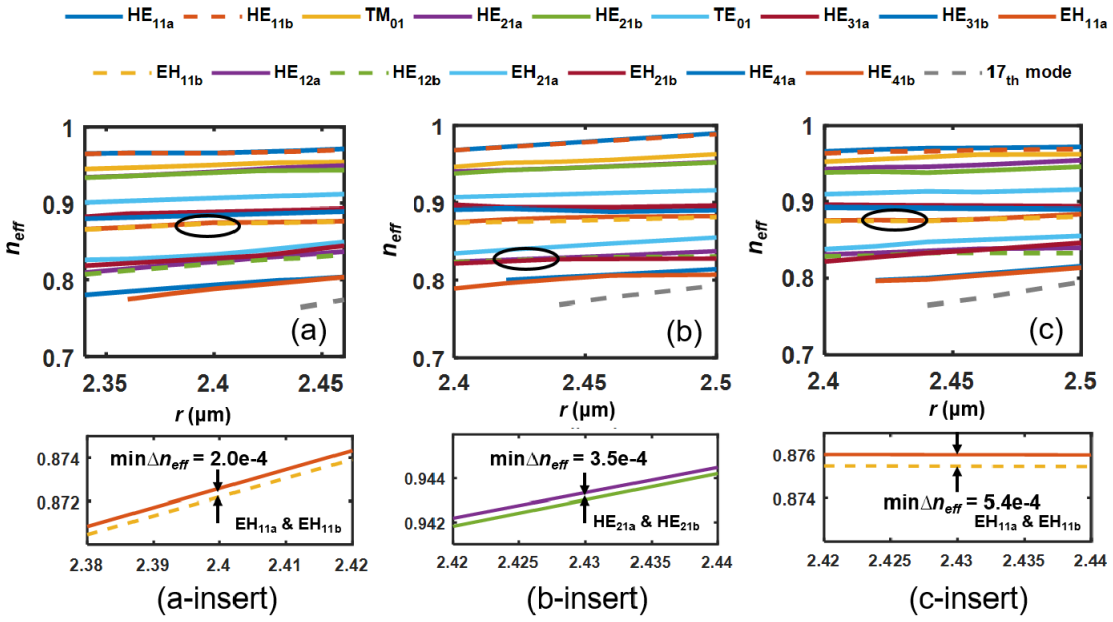

FIGURE 5. Variation of n_{eff} as a function of air core radius r with the periodic layer width l = (a)1.8μm; (b)1.85μm; and (c)1.9μm, when d/r is fixed to be 0.1 and l_1/l is fixed to be 0.33.

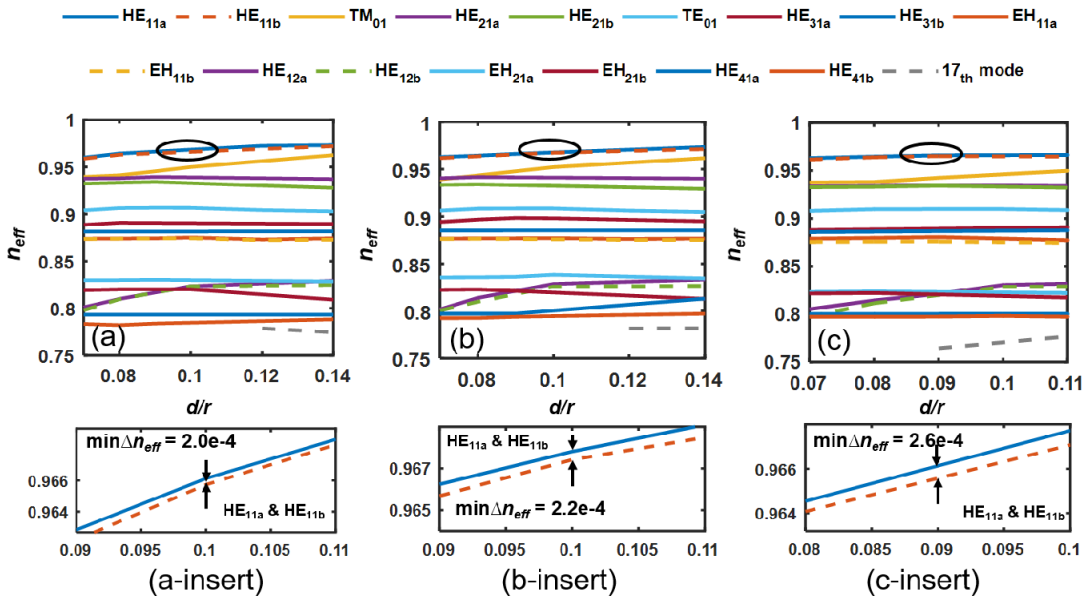

FIGURE 6. Variation of n_{eff} as a function of circular dielectric medium radius/air core radius (d/r) with r = (a)2.4μm; (b)2.42μm; and (c)2.44μm, when l is fixed to be 1.8μm.

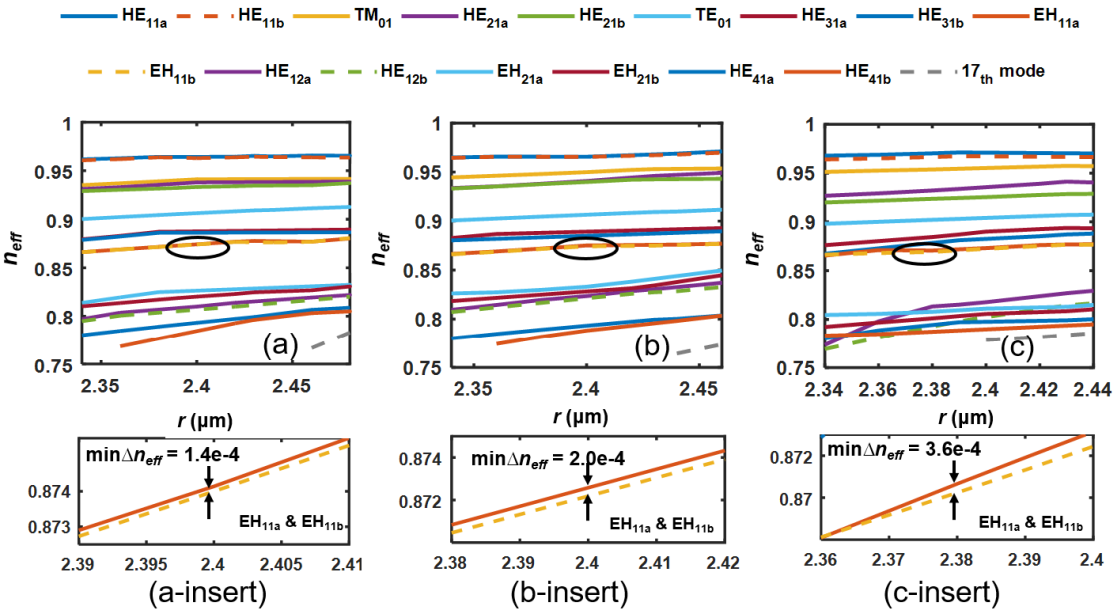

FIGURE 7. Variation of n_{eff} as a function of air core radius r with d/r = (a)0.08; (b)0.1; and (c)0.12, when l is fixed to be 1.8μm.

be 0.33. The curves of adjacent modes with $min\Delta n_{eff}$ are enlarged and inserted at the bottom of Fig. 5. From Fig. 5, the $min\Delta n_{eff}$ changes little when r goes from 2.4 to 2.45, while the 16-mode interval narrows. Among the interval, the $min\Delta n_{eff}$ can always be $> 10^{-4}$. Taking the above into account, we optimize the periodic layer width l to be 1.8($l_1 \approx$ 0.59) as the final design. In this case, r should be less than 2.43μm to avoid the appearance of the 17th propagation mode (TE_{02}).

Figure 6 indicates the variation of n_{eff} as a function of circular dielectric medium radius/air core radius (d/r) with $r = 2.4\mu$m, 2.42μm and 2.44μm, when each periodic layer width l is fixed to be 1.8μm. Figure 7 indicates the variation of n_{eff} as a function of air core radius r with $d/r = 0.08$, 0.1 and 0.12. From Fig. 6, the $min\Delta n_{eff}$ of the required modes increases with d/r increasing, which means the dielectric medium core can effectively separate adjacent modes, also be consistent with the results in Section A. From Fig. 7,

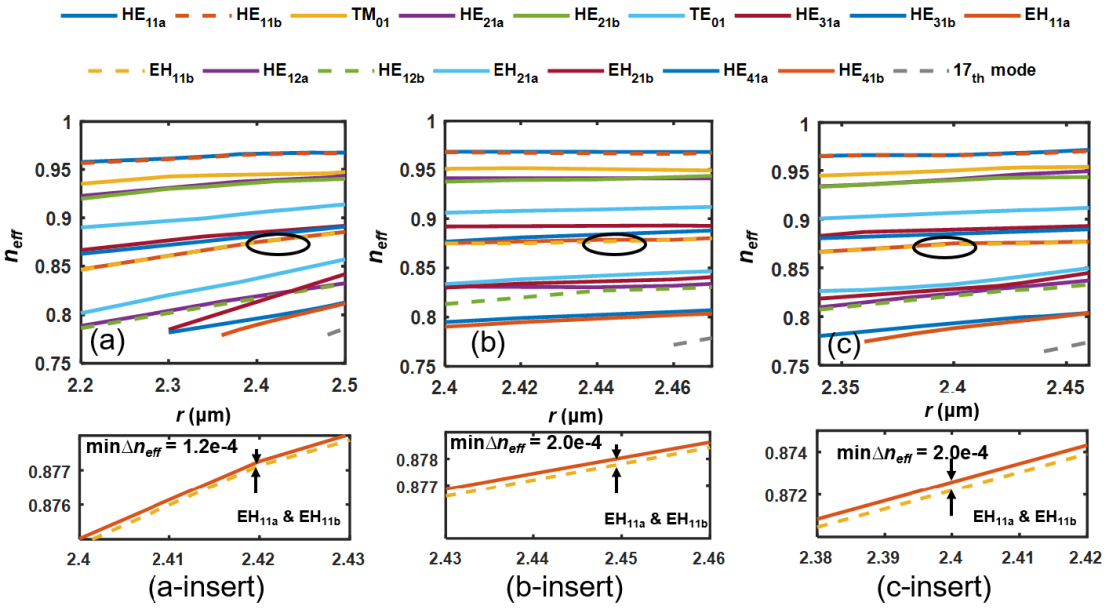

FIGURE 8. Distribution of $min\Delta n_{eff}$ between every two of the desired propagation modes of the proposed fiber. The colored curves indicate the cut-off lines of the 16th mode and the 17th mode.

as r increases, the overall n_{eff} as same as the $min\Delta n_{eff}$ will increase, and the number of propagation modes also increases. Figure 7 indicates that the enlarging of air core size within certain range contributes to the increasing of propagation mode numbers, which is the same as ordinary total reflection fibers. However the rising range is not much for Δn_{eff} when d/r rises from 0.1 to 0.12, and in order to keep 16 modes, either r or d cannot be too large. Taking the fabricating complexity into consideration, we reserve two decimal fractions and choose d/r to be 0.1. In this case, r is chosen to be $\approx 2.4\mu$m. The overall result shows that minor manufacturing differences of the core parameters are permitted among the fault tolerance requirements, and will not influence the modal distance greatly. Both the core and the inner radius of cladding can be made a little larger for larger $min\Delta n_{eff}$ as long as the 16-mode condition is met.

We further study the joint influence of d and r on the values of $min\Delta n_{eff}$. Figure 8 shows the distribution of $min\Delta n_{eff}$ between every two of the desired 16 modes. The vertical axis stands for the air core radius r, and the horizontal axis stands for the proportion of central dielectric medium in the core region d/r. The solid curves correspond to the threshold lines when the number of propagation modes is 16 and $\geq$ 17(or in other words, mode 'cut-off' lines), thereby forming a 16-vector-mode region circled by these curves at the wavelength 1550nm. When the number of propagation spatial modes exceeds 16 with the variation of parameters, Δn_{eff} related to higher-order modes (e.g. Δn_{eff} between HE_{41b} and TE_{02}) are not considered. Also, when some of the desired 16 modes are cut-off, Δn_{eff} related to the certain modes are not considered. So the comparatively large $min\Delta n_{eff}$ can be found in this region. From Fig. 8, when the other parameters are fixed to be constant, the number of modes goes up as r or d/r increases. Also, the overall $min\Delta n_{eff}$ will increase with the increasing of r or d. Compared with r, d/r effects $min\Delta n_{eff}$ more obviously. Though the $min\Delta n_{eff}$ in Fig. 8 all exceed 10^{-4}, the $min\Delta n_{eff}$ change is not evident in the circled region. It's better to choose geometrical parameters set at the right side to gain larger $min\Delta n_{eff}$. For all of the above reasons, we optimize r and d to be 2.4μm and 0.24μm($d/r \approx 0.1$) as the final design.

Figure 9 indicates the variation of Δn_{eff} as a function of air core radius r with $n_c = 4.2$, 4.4, and 4.58, when d/r is fixed to be 0.1. The $min\Delta n_{eff}$ of the required modes increases when n_c gets larger according to Fig. 9, and the appearance of higher-order modes gets earlier. So one can make a high refractive index central core by doping high-index materials to obtain high Δn_{eff} between adjacent modes. We choose the central dielectric medium to be the same material as the high-index cladding layer in our research.

For Bragg fibers, the number of periodic layers determines the capability of light confinement, while the modal confinement loss of the Bragg fiber mainly decides the transmission haul of a certain mode before it fades away. During the above optimization, we use 15 layers. Figure 10(a) indicates the variation of confinement loss as a function of periodic layer numbers when each periodic layer l is fixed to be 1.8μm, and Figure 10(b) shows the enlarged partial of the left bottom in Fig. 10(a). From Fig. 10, the confinement losses of several modes are quite large when the layer numbers $\leq$ 15. When the layer number exceeds 18, the confinement losses of most modes drop to under 10 dB/m and the curves become steady. The maximum loss declines below 1 dB/m when the layer number is more than 25. We optimize the number to be 18 preliminarily.

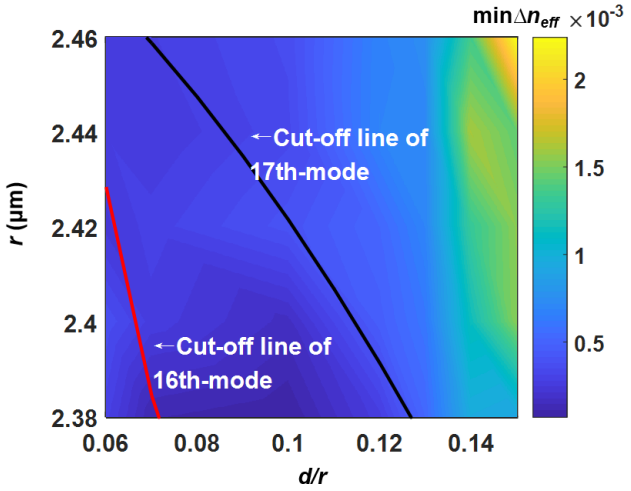

FIGURE 9. Variation of n_{eff} as a function of air core radius r with n_c = (a)4.2; (b)4.4; and (c)4.58, when d/r is fixed to be 0.1.

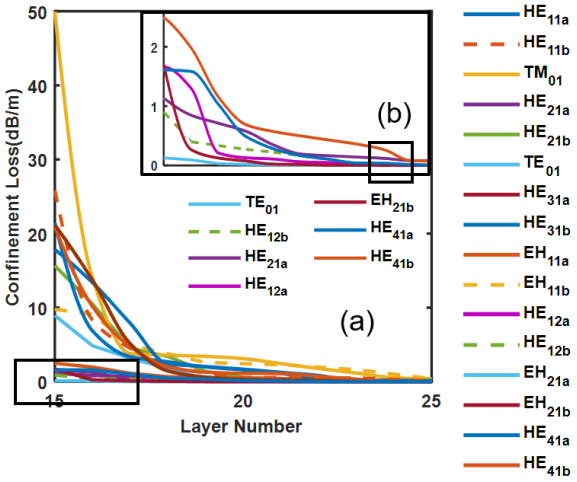

FIGURE 10. The variation of fiber confinement loss as a function of layer number.

In air-core Bragg fibers, the transmission loss L_t can be defined as the sum of confinement loss L_c and absorption loss L_a under relatively ideal conditions (no crosstalk between channels or manufacturing errors):

$$L_t = L_c + L_a \tag{12}$$

The absorption loss coefficient can be obtained by: [35]

$$L_a = \frac{1}{R}\left(\frac{A_{layers}}{A_{core}}\right)^2 \tag{13}$$

where R is the normalized core radius, A_{core} and A_{layers} are the amplitudes of the electric field in the core and cladding layers. Air-core Bragg fibers are supposed to have much smaller absorption loss than ordinary silica fibers [28]. The calculated absorption losses of the proposed fiber are presented in Table 1.

From Table 1, the absorption loss $L_a(< 2.5\text{dB/km})$ is far smaller than the confinement loss $L_c(< 1\text{dB/m})$, so for the proposed fiber, the transmission loss L_t is mainly determined

TABLE 1. The Calculated Absorption Losses of the Proposed Fiber.

Mode	HE_{11a}	HE_{11b}	TM_{01}	HE_{21a}	HE_{21b}	TE_{01}
Loss(dB/km)	0.942	0.974	0.049	0.102	0.107	0.002
Mode	HE_{31a}	HE_{31b}	EH_{11a}	EH_{11b}	HE_{12a}	HE_{12b}
Loss(dB/km)	0.172	0.291	0.053	0.028	2.312	1.350
Mode	EH_{21a}	EH_{21b}	HE_{41a}	HE_{41b}		
Loss(dB/km)	0.042	0.512	0.183	0.954		

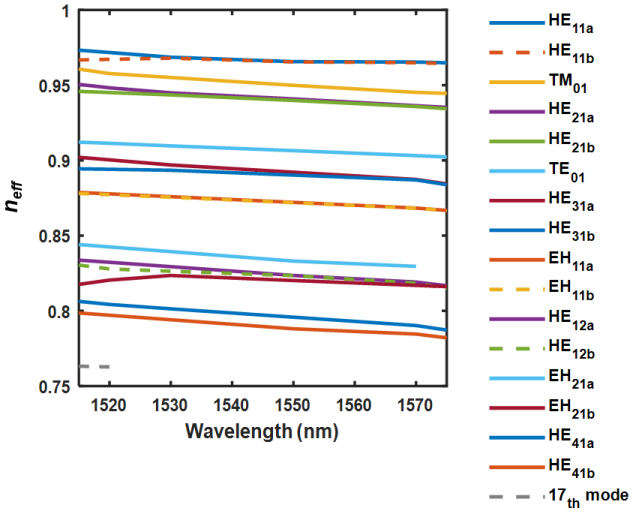

FIGURE 11. The variation of n_{eff} as a function of wavelength/nm.

by L_c. When the number of layers is enough, L_t can be less than 1dB/m.

III. RESULTS

Based on the above design, we choose the parameter of $r = 2.4\mu$m, $d = 0.24\mu$m, $l = 1.8\mu$m and $n_c = 4.58$. We study some of the performance parameters of the proposed fiber, and evaluate the results.

A. WORKING WAVELENGTH

The variation of Δn_{eff} as a function of wavelength is shown in Fig. 11. Results illustrate that the designed fiber works over a range of wavelength from 1520nm to 1570nm, across the whole C-band. Both n_{eff} and Δn_{eff} fall with the wavelength going up, and the number of supporting modes reduces. At 1570nm, $min\Delta n_{eff}$ turns to be 0.00012, which is also acceptable.

B. MODE EFFECITVE AREA

The mode effective area(A_{eff}) of fibers determines their properties of nonlinearity impairment limitation. As for the proposed fiber, the A_{eff} is not supposed to be too large as the geometrical size of the fiber is small. We compute A_{eff} by [35]:

$$A_{eff} = \frac{(\iint |E|^2 dxdy)^2}{\iint |E|^4 dxdy} \tag{14}$$

The variation tendency of the minimal and maximal A_{eff} under the influence of varying r and d/r are shown in Fig. 12(a) and 12(b) separately. Based on Fig. 12(a) and 12(b), the A_{eff} among the 16 propagation

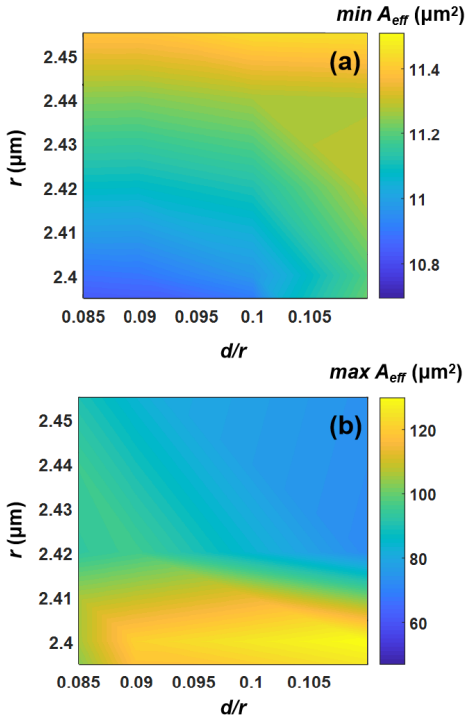

FIGURE 12. The variation of A_{eff} as function of r and d/r. (a) The $min(A_{eff})$; (b) The $max(A_{eff})$.

modes can be varied from 10 to 130μm^2. The $min(A_{eff})$ of the proposed fiber is around 11μm^2, and its value tends to increase a little with the enlarging of r and d. On the other hand, when r or d gets higher, the $max(A_{eff})$ gets smaller in the given interval. Of all the 16 vector modes, when the air core radius r is set to be 2.4μm and d/r is set to be 0.1, TE_{01} has the lowest A_{eff} of 10.97 μm^2 and HE_{31a} has the highest A_{eff} of 130.08 μm^2. Other results are shown in Table 2 at the bottom.

C. DIFFERENTIAL MODE DELAY

For short-haul transmission systems, the computation complexity and power consumption can be measured by the differential mode delay(DMD), which is critical for simplifying or eliminating the MIMO DSP in the receiver end. DMD between two adjacent modes can be defined as the value of subtracting the group delay τ_A of τ_B, which is expressed as follows [2]:

$$DMD = \tau_B - \tau_A = \frac{n_{gB} - n_{gA}}{c} = \frac{n_{effB} - n_{effA}}{c} - \frac{\lambda}{c}\left(\frac{\partial n_{effB}}{\partial \lambda} - \frac{\partial n_{effA}}{\partial \lambda}\right) \quad (15)$$

where τ_i represents the group delay of two modes, n_{gi} represents the group indices, c is the light velocity in a vacuum and λ means the free space wavelength. Figure 13 shows the variation of DMD as a function of wavelength, with all the other design parameters set as the values above. As shown in Fig. 13, the DMD between all adjacent modes $<$ 5ns/m. The actual calculated results of DMD for the designed Bragg fiber are shown in Table 2, with all the other characteristics.

TABLE 2. The Optimized Modal Properties of the 16 Desired Modes at 1550nm. The Δn_{eff} and DMD are Between Adjacent Modes.

Mode	HE_{11a}	HE_{11b}	TM_{01}	HE_{21a}
Mode field distribution				
n_{eff}	0.9657	0.9655	0.9500	0.9409
Δn_{eff}	-	0.0002	0.0155	0.0091
A_{eff}(μm^2)	14.76	14.37	21.03	23.89
DMD (ns/m)	-	0.12	2.12	0.80
Mode	HE_{21b}	TE_{01}	HE_{31a}	HE_{31b}
Mode field distribution				
n_{eff}	0.9399	0.9065	0.8966	0.8926
Δn_{eff}	0.0010	0.0334	0.0099	0.0040
A_{eff}(μm^2)	14.41	10.97	130.08	86.61
DMD (ns/m)	1.35	0.47	4.15	0.14
Mode	EH_{11a}	EH_{11b}	HE_{12a}	HE_{12b}
Mode field distribution				
n_{eff}	0.8752	0.8744	0.8236	0.8234
Δn_{eff}	0.0174	0.0008	0.0508	0.0002
A_{eff}(μm^2)	114.72	87.81	94.61	97.71
DMD (ns/m)	0.18	0.11	1.98	1.86
Mode	EH_{21a}	EH_{21b}	HE_{41a}	HE_{41b}
Mode field distribution				
n_{eff}	0.8331	0.8202	0.7932	0.7881
Δn_{eff}	0.0097	0.0129	0.0270	0.0051
A_{eff}(μm^2)	20.83	27.56	14.26	13.95
DMD (ns/m)	1.11	2.09	2.13	1.95

D. BENDING LOSS ANALYSIS

The bending effect can be determined due to different modes' field distributions and propagation constants. In order to contain more high-order modes in the proposed FMF, the bending loss performance is influenced by the confinement loss to some content. By calculating the imaginary part of fiber effective mode index $Im(n_{eff})$, fiber bending loss of each mode can be obtained by formula (1) in 3.1. In calculations,

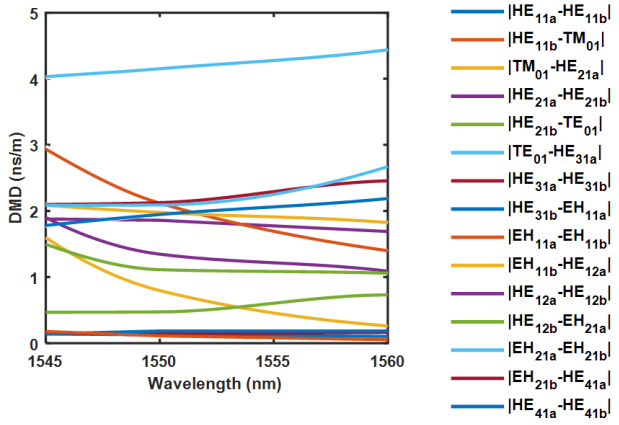

FIGURE 13. Variation of DMD as a function of wavelength(nm).

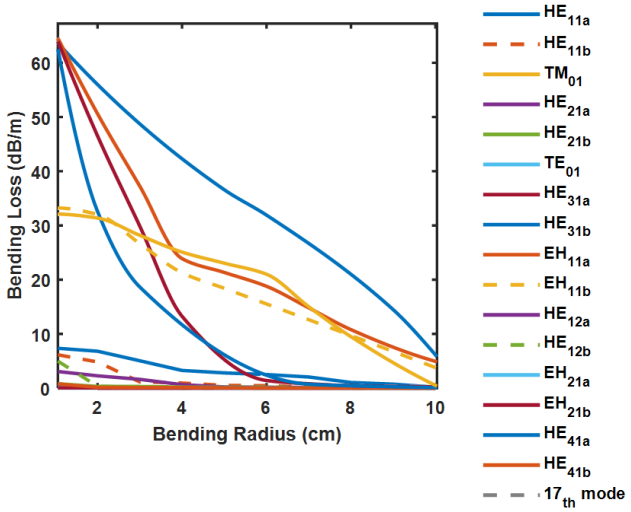

FIGURE 14. The variation of bending loss as a function of bending radius *R*.

the bending equivalent refractive index is computed by [37]:

$$n(x, y) = n_0(x, y)(1 + x/R) \tag{16}$$

The variation of loss as a function of fiber bending radius R is shown in Fig. 14. The fiber is bent towards the horizontal axis of the cross section. It can be acquired that modes with higher confinement loss are easier to fade out while bending. According to Fig. 14, when the bending radius is more than 10cm, the bending losses of each mode are below 10 dB/m. At the bending radius of 1mm, the bending losses of 10 modes are less than 10dB/m. When bending radius is small, losses of higher-order modes are more sensitive to the bending radius, while also influenced by the confinement ability. The bending loss as well as the confinement loss will decrease when the number of cladding layers is large enough.

The final optimized modal properties of the 16 desired modes are shown in Table 2. We achieve large $min\Delta n_{eff}$ of $\sim 2 \times 0.0001$ as the final design. Comparing with the conventional FMFs, the proposed fiber structure can greatly improve the transmission capacity of the communication system by making full use of eigenmodes, as the conventional FMFs mainly support LP modes [37] and their mode groups are not fully utilized [38]. Though the few-mode Bragg fibers are not as easily to be fabricated as ordinary FMFs, they have a good prospect of being applied in MDM systems.

IV. CONCLUSION

In conclusion, the proposed weakly-coupled coaxial Bragg fiber supporting 16 vector modes(HE_{11a}, HE_{11b}, TM_{01}, HE_{21a}, HE_{21b}, TE_{01}, HE_{31a}, HE_{31b}, EH_{11a}, EH_{11b}, HE_{12a}, HE_{12b}, EH_{21a}, EH_{21b}, HE_{41a}, HE_{41b}) can achieve large $min\Delta n_{eff}$ of $\sim 2 \times 0.0001$ between adjacent modes at 1550nm, and works across the C-band. Numerical simulations are carried out on n_{eff}, $min\Delta n_{eff}$ and A_{eff} to investigate the influence of geometric parameters within the regions that meet the 16-vector-mode design condition. The DMD, modal confinement loss and bending effect are also evaluated. Simulation results show that the coaxial structure can effectively split adjacent eigenmodes, and reveal the possibility for weakly-coupled Bragg FMFs for short-haul communications.

REFERENCES

[1] G. Li, M. Karlsson, X. Liu, and Y. Quiquempois, "Focus issue introduction: Space-division multiplexing," *Opt. Exp.*, vol. 22, no. 26, pp. 32526–32527, 2014.
[2] M. Kasahara, K. Saitoh, T. Sakamoto, N. Hanzawa, T. Matsui, K. Tsujikawa, and F. Yamamoto, "Design of three-spatial-mode ring-core fiber," *J. Lightw. Technol.*, vol. 32, no. 7, pp. 1337–1343, Apr. 2014.
[3] Y. Xie, L. Pei, J. Zheng, Q. Zhao, T. Ning, and J. Sun, "Design and analysis of a combined-ring core weakly coupled few-mode fiber with six linearly polarized modes and an ultra-large effective index difference," *Appl. Opt.*, vol. 58, no. 16, pp. 4373–4380, 2019.
[4] A. Corsi, J. H. Chang, L. A. Rusch, and S. LaRochelle, "Design of highly elliptical core ten-mode fiber for space division multiplexing with 2 × MIMO," *IEEE Photon. J.*, vol. 11, no. 2, pp. 1–10, Apr. 2019.
[5] S. Chen and J. Wang, "Fully degeneracy-lifted bow-tie elliptical ring-core multi-mode fiber," *Opt. Exp.*, vol. 26, no. 14, pp. 18773–18782, 2018.
[6] P. Yeh, A. Yariv, and E. Marom, "Theory of Bragg fiber," *J. Opt. Soc. Amer.*, vol. 68, no. 9, pp. 1196–1201, Sep. 1978.
[7] W. Zhi, R. Guobin, L. Shuqin, L. Weijun, and S. Guo, "Compact supercell method based on opposite parity for Bragg fibers," *Opt. Exp.*, vol. 11, no. 26, pp. 3542–3549, 2003.
[8] S. Guo, F. Wu, K. Ikram, and S. Albin, "Analysis of circular fibers with an arbitrary index profile by the Galerkin method," *Opt. Lett.*, vol. 29, no. 1, pp. 32–34, 2004.
[9] G. Ouyang, Y. Xu, and A. Yariv, "Comparative study of air-core and coaxial Bragg fibers: Single-mode transmission and dispersion characteristics," *Opt. Exp.*, vol. 9, no. 13, pp. 733–747, 2001.
[10] Y. Xu, G. X. Ouyang, R. K. Lee, and A. Yariv, "Asymptotic matrix theory of Bragg fibers," *J. Lightw. Technol.*, vol. 20, no. 3, pp. 428–440, Mar. 2002.
[11] J.-I. Sakai and P. Nouchi, "Propagation properties of Bragg fiber analyzed by a Hankel function formalism," *Opt. Commun.*, vol. 249, nos. 1–3, pp. 153–163, May 2005.
[12] M. Jelinek, V. Kubecek, H. Jelinkova, V. Matejec, I. Kasik, and O. Podrazky, "Experimental investigation of high power picosecond 1.06 μm pulse propagation in Bragg fibers," *Proc. SPIE*, vol. 8772, no. 1, pp. 188–197, 2013.
[13] J. Sakai, "Hybrid modes in a Bragg fiber: General properties and formulas under the quarter-wave stack condition," *J. Opt. Soc. Amer. B, Opt. Phys.*, vol. 22, no. 11, pp. 2319–2330, 2005.
[14] M. Miyagi, A. Hongo, Y. Aizawa, and S. Kawakami, "Fabrication of germanium-coated nickel hollow waveguides for infrared transmission," *Appl. Phys. Lett.*, vol. 43, no. 5, pp. 430–431, 1983.
[15] H. Ito, T. Nakata, K. Sakaki, M. Ohtsu, K. I. Lee, and W. Jhe, "Laser spectroscopy of atoms guided by evanescent waves in micron-sized hollow optical fibers," *Phys. Rev. Lett.*, vol. 76, no. 24, pp. 4500–4503, Jun. 1996.

[16] Y. Fink, D. J. Ripin, S. Fan, C. Chen, J. D. Joannopoulos, and E. L. Thomas, "Guiding optical light in air using an all-dielectric structure," *J. Lightw. Technol.*, vol. 17, no. 11, pp. 2039–2041, Nov. 1999.

[17] R. F. Cregan, B. J. Mangan, J. C. Knight, T. A. Birks, P. J. S. Russell, P. J. Roberts, and D. C. Allan, "Single-mode photonic band gap guidance of light in air," *Science*, vol. 285, no. 5433, pp. 1537–1539, 1999.

[18] T. Engeness, M. Ibanescu, S. G. Johnson, O. Weisberg, M. Skorobogatiy, S. Jacobs, and Y. Fink, "Dispersion tailoring and compensation by modal interactions in OmniGuide fibers," *Opt. Exp.*, vol. 11, no. 10, pp. 1175–1196, 2003.

[19] B. Hong, N. Somjit, J. Cunningham, and I. Robertson, "High-order operating mode selection using second-order bandgap in THz Bragg fiber," in *Proc. 10th UK-Eur.-China Workshop Millimetre Waves Terahertz Technol. (UCMMT)*, Liverpool, U.K., Sep. 2017, pp. 1–2.

[20] D. Chen, T. J. Yang, J. J. Wu, L. Shen, K. L. Liao, and S. He, "Band-rejection fiber filter and fiber sensor based on a Bragg fiber of transversal resonant structure," *Opt. Exp.*, vol. 16, no. 21, pp. 16489–16495, 2008.

[21] Y. Wang, G. Yan, Z. Lian, C. Wu, and S. He, "Liquid-level sensing based on a hollow core Bragg fiber," *Opt. Exp.*, vol. 26, no. 17, pp. 21656–21663, 2018.

[22] L. Shang and S. Feng, "Liquid-filled hollow core Bragg fiber sensors using different bandgaps for high-refractive-index sensing," *IEEE Photon. J.*, vol. 11, no. 4, pp. 1–13, Aug. 2019.

[23] D. Gaponov, S. Février, M. Devautour, P. Roy, M. Likhachev, S. Aleshkina, M. Salganskii, M. Yashkov, and A. Guryanov, "Management of the high-order mode content in large (40 μm) core photonic bandgap Bragg fiber laser," *Opt. Lett.*, vol. 35, no. 13, pp. 2233–2235, 2010.

[24] J.-P. Yehouessi, O. Vanvincq, A. Cassez, M. Douay, Y. Quiquempois, G. Bouwmans, and L. Bigot, "Extreme large mode area in single-mode pixelated Bragg fiber," *Opt. Exp.*, vol. 24, no. 5, pp. 4761–4770, 2016.

[25] L. Shang and S. Feng, "Highly-birefringent solid-core Bragg fiber with a high-index-contrast cladding," in *Proc. 18th Int. Conf. Opt. Commun. Netw. (ICOCN)*, Huangshan, China, Aug. 2019, pp. 1–3.

[26] X. Bai, H. Chen, Y. Zhuang, and H. Cao, "A new type Bragg fiber for supporting 50 orbital angular momentum modes," *Optik*, vol. 219, no. 16, p. 5153, 2020.

[27] M. Ibanescu, Y. Fink, S. Fan, E. L. Thomas, and J. D. Joannopoulos, "An all-dielectric coaxial waveguide," *Science*, vol. 289, no. 5478, pp. 415–419, 2000.

[28] S. G. Johnson, M. Ibanescu, M. Skorobogatiy, O. Weisberg, T. D. Engeness, M. Soljacic, S. A. Jacobs, J. D. Joannopoulos, and Y. Fink, "Low-loss asymptotically single-mode propagation in large-core OmniGuide fibers," *Opt. Exp.*, vol. 9, no. 13, pp. 748–779, 2001.

[29] Y. Fink, J. N. Winn, S. Fan, C. Chen, J. Michel, J. D. Joannopoulos, and E. L. Thomas, "A dielectric omnidirectional reflector," *Science*, vol. 282, no. 5394, pp. 1679–1682, 1998.

[30] Y. Xu, R. K. Lee, and A. Yariv, "Asymptotic analysis of Bragg fibers," *Opt. Lett.*, vol. 25, no. 24, pp. 1756–1758, 2000.

[31] Y. Xu, R. K. Lee, and A. Yariv, "Asymptotic analysis of dielectric coaxial fibers," *Opt. Lett.*, vol. 27, no. 12, pp. 1019–1021, 2002.

[32] L. Wang and S. L. Rochelle, "Design of eight-mode polarization-maintaining few-mode fiber for multiple-input multiple-output-free spatial division multiplexing," *Opt. Lett.*, vol. 40, no. 24, pp. 5846–5849, 2015.

[33] S. Février, R. Jamier, and J.-M. Blondy, "Low-loss single-mode large mode area all-silica photonic bandgap fiber," *Opt. Exp.*, vol. 14, no. 2, pp. 562–569, 2006.

[34] J. Han, G. Gao, Y. Zhao, and S. Hou, "Bend performance analysis of few-mode fibers with high modal multiplicity factors," *J. Lightw. Technol.*, vol. 35, no. 13, pp. 2526–2534, Jul. 1, 2017.

[35] A. Kobyakov, S. Kumar, D. Q. Chowdhury, A. B. Ruffin, M. Sauer, S. R. Bickham, and R. Mishra, "Design concept for optical fibers with enhanced SBS threshold," *Opt. Exp.*, vol. 13, no. 14, pp. 5338–5346, 2005.

[36] R. T. Schermer and J. H. Cole, "Improved bend loss formula verified for optical fiber by simulation and experiment," *IEEE J. Quantum Electron.*, vol. 43, no. 10, pp. 899–909, Oct. 2007.

[37] S. Jiang, L. Ma, Z. Zhang, X. Xu, S. Wang, J. Du, C. Yang, W. Tong, and Z. He, "Design and characterization of ring-assisted few-mode fibers for weakly coupled mode-division multiplexing transmission," *J. Lightw. Technol.*, vol. 36, no. 23, pp. 5547–5555, Dec. 1, 2018.

[38] R. Ryf *et al.*, "High-spectral-efficiency mode-multiplexed transmission over graded-index multimode fiber," in *Proc. Eur. Conf. Opt. Commun. (ECOC)*, Rome, Italy, 2018, pp. 1–3.

YIYING ZHANG received the bachelor's degree in communication engineering from the University of Science and Technology Beijing, Beijing, China, in 2015, where she is currently pursuing the Ph.D. degree with the School of Computer & Communication Engineering. Her research interest includes optical communications.

FANG REN received the bachelor's and master's degrees in electronic science and technology from Tianjin University, Tianjin, China, in 2008 and 2010, respectively, and the Ph.D. degree in information electronics from Hokkaido University, Sapporo, Japan, in 2014. Her research interests include optical communication systems, optical devices, and deep learning.

XIAOJIE FAN received the bachelor's degree in communication engineering from the University of Science and Technology Beijing, Beijing, China, in 2017, where he is currently pursuing the Ph.D. degree with the School of Computer & Communication Engineering. His research interests include optical communication and deep learning.

JINYU ZHANG received the bachelor's degree in communication engineering from the University of Science and Technology Beijing, Beijing, China, in 2019, where she is currently pursuing the master's degree with the School of Computer & Communication Engineering. Her research interests include optical devices and transmission waveguides.

JINGJING NIU received the bachelor's degree in communication engineering from the University of Science and Technology Beijing, Beijing, China, in 2019, where she is currently pursuing the master's degree with the School of Computer & Communication Engineering. Her research interest includes optical communications.

JIANPING WANG received the bachelor's, master's, and Ph.D. degrees from the School of Precision Instrument & Optoelectronic Engineering, Tianjin University, Tianjin, China, in 1995, 1997, and 2000, respectively. Her research interests include optical communications, microwave photonics, and deep learning.